

# Contrastive Principal Component Learning: Modeling Similarity by Augmentation Overlap

Lu Han, Han-Jia Ye, De-Chuan Zhan

State Key Laboratory for Novel Software Technology

Nanjing University

Nanjing, 210023, China.

{hanlu, yehj, zhandc}@lamda.nju.edu.cn

## Abstract

Traditional self-supervised contrastive learning methods learn embeddings by pulling views of the same sample together and pushing views of different samples away. Since views of a sample are usually generated via data augmentations, the semantic relationship between samples is ignored. Based on the observation that semantically similar samples are more likely to have similar augmentations, we propose to measure similarity via the *distribution* of augmentations, *i.e.*, how much the augmentations of two samples overlap. To handle the dimensional and computational complexity, we propose a novel Contrastive Principal Component Learning (CPCL) method composed of a contrastive-like loss and an on-the-fly projection loss to efficiently perform PCA on the *augmentation feature*, which encodes the augmentation distribution. By CPCL, the learned low-dimensional embeddings theoretically preserve the similarity of augmentation distribution between samples. Empirical results show our method can achieve competitive results against various traditional contrastive learning methods on different benchmarks.

## 1 Introduction

In recent years, the rapid development of contrastive learning has pushed self-supervised representation learning to unprecedented success. Many of the contrastive learning methods surpass traditional pretext-based methods by a large margin and even outperform representation learned by supervised learning [1–7]. The key idea of contrastive learning is to construct views of samples via modern data augmentations [5]. Then discriminative embeddings are learned by pulling together views of the same sample in the embedding space and pushing apart views of others.

Traditional self-supervised contrastive learning methods only utilize the semantic invariance between views of the same sample, but ignore the semantic relationship between samples and push many “false negative” samples [8]. Despite the possible drawbacks, their learned embeddings somehow form semantically meaningful clusters [4–7]. Some of the previous works explain this phenomenon with the strong assumption that two views are conditionally independent given the label or a hidden variable [9, 10]. HaoChen et al. [11] turn the assumption towards how views of different samples are connected by the augmentation process. Wang et al. [12] notice that the augmentation overlap provides a ladder for gradually learning class-separated representations. These analyses motivate us to rethink the role of augmentation and propose a better way of exploiting the ability of augmentation.

In this paper, we provide a new way of constructing self-supervised contrastive learning tasks. We observe that modern augmentation methods tend to have similar augmentation results if two samples are semantically similar. As is shown in Figure 1 left, two pictures of deer can create many similar crops, *i.e.*, their augmentation distributions overlap much. In contrast, a car image can not be augmented to the same crop as a deer, and their augmentation distributions overlap little. In Figure 1 right, we also use the classical image matching [13] algorithm to estimate how much intra- and inter-class samples overlap on common datasets. By counting the portion of matched key points, we find samples of the same class overlap more than different classes, which supports our motivation. Therefore, we establish the relationship between samples based on the similarity of their augmentation distributions, *i.e.*, how much they overlap.

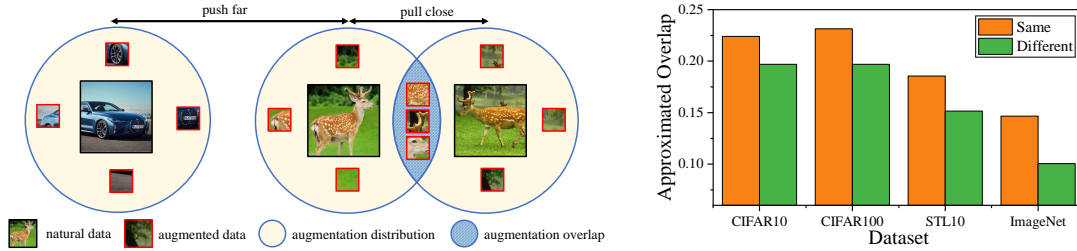


Figure 1: Modern augmentation methods usually create similar augmentations for samples with semantically the same class. The right figure shows the averaged overlap between samples with the same and different classes on common datasets. For this reason, we model the similarity of two natural data by how much their augmentation distributions overlap. Then self-supervised learning tasks can be constructed with the objective of preserving such similarity.

However, the similarity (or distance) between augmentation distributions is usually difficult or impractical to compute directly, especially when the data lie in high dimensional space. Therefore, we employ the idea of PCA [14] to perform dimension reduction on a special feature representation called *augmentation feature*, which encodes the augmentation information. To handle the dimensional and computational complexity, we propose a novel Contrastive Principal Component Learning (CPCL) method that utilizes a contrastive-like loss to learn principal components and an on-the-fly projection loss to map the data to low dimensional space. Via CPCL, the learned embeddings can theoretically preserve the sample-wise augmentation distribution distances.

The similarity between our loss and traditional contrastive loss may explain why the traditional contrastive methods can learn semantic-related embeddings – they embed the samples into spaces that preserve how similar their augmentation is. Experiments on both synthetic and real-world data show our method can achieve competitive results against various traditional contrastive learning methods. Our contributions are:

- We propose a new way of constructing contrastive learning tasks by measuring the similarity of augmentation distributions between two samples. Then we learn embeddings to preserve this similarity.
- We propose Contrastive Principal Component Learning (CPCL) by employing the idea of PCA on augmentation feature which encodes information about the augmentation distributions. As a result, the learned embeddings preserve augmentation similarity between samples.
- Our CPCL contains traditional contrastive loss as a part, which may explain the functionality of contrastive learning and why they can learn semantic meaningful embeddings.

## 2 Related Work

**Self-Supervised learning.** Learning effective visual representations without human supervision is a long-standing problem. Self-supervised learning methods solve this problem by creating supervision from the data itself instead of human labelers. The model needs to solve a pretext task before it is used for the downstream tasks. For example, in computer vision, the pretext tasks include colorizing grayscale images [15], inpainting images [16], predicting relative patch [17], solving jigsaw puzzles [18], predicting rotations [19] and exploiting generative models [20–22]. Similarly, in natural language processing, self-supervised learning also achieves great success [23, 24].

**Contrastive Learning.** Contrastive approaches have been one of the most prominent representation learning strategies in self-supervised learning. The idea behind these approaches is to maximize the agreement between positive pairs and minimize the agreement between negative pairs. Positive pairs are commonly constructed by co-occurrence [2, 3, 25] or augmentation of the same sample [4–7, 26], while all the other samples are taken as negatives. Most of these methods employ the InfoNCE loss [2] which acts as a lower bound of mutual information. Some methods do not involve negative samples and

use other mechanisms to prevent collapse [27, 28]. However, these methods only utilize the semantic invariance of augmentation but ignore the relationship between samples.

**Explanation of Contrastive Learning.** Several works provide empirical or theoretical results for explaining the behavior of contrastive learning. Tian et al. [29], Xiao et al. [30] explore the role of augmentation and show contrastive model can extract useful information from views but also can be affected by nuisance information. Zhao et al. [31] empirically shows that contrastive learning preserves low-level or middle-level instance information. In theoretical studies, Saunshi et al. [9] provide guarantees of downstream linear classification tasks under conditionally independence assumption. Other works weaken the assumption but are still unrealistic [32, 10]. HaoChen et al. [11] focus on how views of different samples are connected by the augmentation process and provide guarantees with certain connectivity assumptions. Wang et al. [12] notice that the augmentation overlap provides a ladder for gradually learning class-separated representations. However, Wang et al. [12] provides their analysis based on the assumption that common contrastive loss can somehow learn to align overlapped samples. In contrast, we provide a novel contrastive method that ensures preserving augmentation overlap.

### 3 Notations and Preliminary

Denote the set of all the natural data (the data without augmentation) as  $\bar{\mathcal{X}}$ , with its size  $|\bar{\mathcal{X}}| = N$ . We assume the natural data follows a uniform distribution  $p(\bar{x})$  on  $\bar{\mathcal{X}}$ , i.e.,  $p(\bar{x}) = \frac{1}{N}, \forall \bar{x} \in \bar{\mathcal{X}}$ . Given an augmentation method  $\mathcal{A}$ , the augmentation distribution of a natural sample  $\bar{x} \in \bar{\mathcal{X}}$  is  $p_{\mathcal{A}}(\cdot|\bar{x})$  (we omit the subscript  $\mathcal{A}$  and directly use  $p(\cdot|\bar{x})$  in the following content for convenient).<sup>1</sup> For example, if  $\bar{x}$  is an image, then  $\mathcal{A}$  can be common augmentations like Gaussian blur, color distortion and random cropping [5]. We can get augmented data by applying  $\mathcal{A}$  to samples from  $\bar{\mathcal{X}}$ , and the set of all possible augmented data is  $\mathcal{X}$ . We Assume  $\mathcal{X}$  has finite size  $|\mathcal{X}| = L$  and  $L > N$  for ease of exposition. Note that  $N$  and  $L$  are finite but they can be arbitrarily large.

Self-Supervised representation Learning (SSL) extracts features with an encoder  $f_{\theta}$ , parameterized by  $\theta$ , which projects a sample  $x$  to an embedding vector in  $\mathbb{R}^k$ . By training on a pretext task, the goal of SSL is to acquire an encoder to perform well on various kinds of downstream tasks. Traditional contrastive learning tasks use augmentation to create views, taking advantage of its semantic invariance property. They pull views of the same samples together and push away views of different samples. A common practice is to use a contrastive loss, e.g, the InfoNCE loss [2]:

$$\mathcal{L}_{\text{InfoNCE}} = -\mathbb{E}_{x, x^+} f(x)^{\top} f(x^+) + \mathbb{E}_{x, \{x^-\}} \log \sum_{x^-} e^{f(x)^{\top} f(x^-)}. \quad (1)$$

Since any two different samples are pushed away, these methods ignore the relationship between samples and can not explain how to learn semantically meaningful representations. Different from them, we propose a new way to perform contrastive learning with the observation that there exists a strong correlation between the similarity of *augmentation distributions* and the similarity of semantics.

### 4 Learning via Augmentation Overlap

As we mentioned in Section 1, measuring the similarity between augmentation distributions, i.e, the overlap of augmented distributions, reveals the *semantic* relationship between samples well. For example, in natural language processing, we usually generate augmented sentences by dropping out some words. Then different sentences with similar meanings are likely to contain the same set of words and thus have a high probability of creating similar augmented data. Therefore, we formulate the embedding learning task aiming to meet the following similarity preserving condition:

$$d_{\mathbb{R}^k}(f_{\theta^*}(\bar{x}_1), f_{\theta^*}(\bar{x}_2)) \propto d_{\mathcal{A}}(p(\cdot|\bar{x}_1), p(\cdot|\bar{x}_2)). \quad (2)$$

$d_{\mathbb{R}^k}$  is a distance measure in the embedding space  $\mathbb{R}^k$ , and  $d_{\mathcal{A}}$  measures the distance between two augmentation distributions. Equation (2) requires the learned embedding with the optimal parameter  $\theta^*$

<sup>1</sup>Note that  $p(\cdot|\bar{x})$  is usually difficult to compute and we can only sample from it.

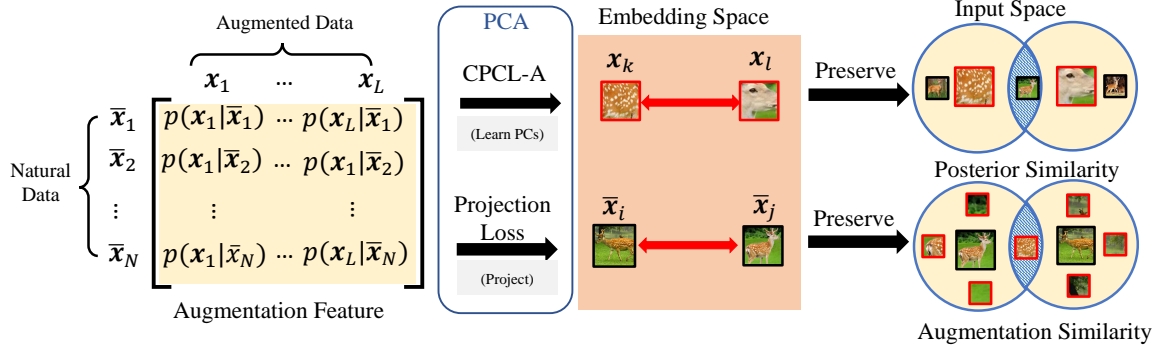


Figure 2: The idea of learning embeddings via Contrastive Principal Component Learning (CPCL). CPCL performs PCA on the augmentation feature, which encodes all the information about the augmentation distribution. By optimizing CPCL loss, which consists of CPCL-A and projection loss, our model can learn embeddings that preserve posterior similarity for augmented data and augmentation similarity for natural data.

has the *same similarity comparison* with that measured by the augmentation distributions. A naive way to implement such embedding property is using a co-called augmentation feature.

#### 4.1 Augmentation Feature

To reach the goal of similarity preserving Equation (2), a direct way is to construct the feature by the augmentation distributions of each natural samples, *i.e.*,  $f_{\theta^*}(\bar{x}) = [p(\mathbf{x}_1|\bar{x}), \dots, p(\mathbf{x}_L|\bar{x})]^\top$ , where each element  $p(\mathbf{x}_i|\bar{x})$  represent the probability of getting  $\mathbf{x}_i$  by augmenting  $\bar{x}$ . In this case, any distance  $d_{\mathbb{R}^L}$  defined in space of  $f_{\theta^*}$  is exactly the valid distribution distance  $d_A$ . We call feature of this kind *augmentation feature*. Though augmentation feature satisfies the similarity preserving condition (Equation (2)) without loss of information, it is impractical for the following reasons. First, its dimensionality is exponentially high, which is up to  $L$ , the number of possible augmented results. Second, the computation of each element is intractable. We may need an exponentially large number of samples to accurately estimate each  $p(\mathbf{x}|\bar{x})$ . The dimensionality and computation problems make augmentation feature impractical both at inference and training time. Such inconvenience motivates us to conduct certain dimension reduction to preserve the information in low dimensional space and develop an efficient algorithm for it. In this paper, we propose Contrastive Principal Component Learning (CPCL) that can efficiently perform dimension reduction on a transformed version of augmentation feature.

#### 4.2 Contrastive Principal Component Learning

Contrastive Principal Component Learning (CPCL) employs the idea of PCA [14], which preserve the reconstruction of data.<sup>2</sup> For convenient, we denote the design matrix of augmentation feature by  $A$ , where  $A \in \mathbb{R}^{N \times L}$ ,  $A_{\bar{x}, \mathbf{x}} = p(\mathbf{x}|\bar{x})$  (see Figure 2). CPCL performs PCA on a transformed augmentation feature called *normalized augmentation feature*:

$$\hat{A} = AD^{-\frac{1}{2}} \quad (3)$$

where  $D = \text{diag}([d_{\mathbf{x}_1}, d_{\mathbf{x}_2}, \dots, d_{\mathbf{x}_L}])$ ,  $d_{\mathbf{x}} = \sum_{\bar{x}} p(\mathbf{x}|\bar{x})$ . Using the transformed augmentation feature leads to two benefits. First,  $d_{\mathbf{x}}$  measures the relative frequent of getting each augmented data when we augment randomly sampled natural data. The background is usually ubiquitous and unimportant, with large  $d_{\mathbf{x}}$ . Normalized augmentation feature will down-weight the elements at augments from background. So it focuses on the main objects, which contribute more with small  $d_{\mathbf{x}}$ . Second, more importantly, based on normalized augmentation feature, we can develop an efficient algorithm for similarity preserving embeddings.

<sup>2</sup>In this paper, we use the non-centered version [33], which is more appropriate for observations than for variables, where the origin matters more.

**The PCA process.** Assume the SVD of  $\hat{A} = U\Sigma V^\top$ , PCA first learns the projection matrix consisting of the top- $k$  right singular vectors, which can be denoted as  $\tilde{V}$ . The vectors in  $\tilde{V}$  are called Principal Components (PCs). Then, it projects the feature by  $\hat{A}\tilde{V}$  to get the embeddings for each sample. Performing PCA on the augmentation feature will encounter many obstacles. First, the element of augmentation feature is not possible to accurately estimate. Second, even though we can somehow get the precise value of each  $p(\mathbf{x}|\bar{\mathbf{x}})$ , the augmentation feature is exponentially large, making the PCA process too time-consuming. Third, assume we can somehow get the projection matrix  $\tilde{V}$ , it is also impractical to project high dimensional matrix  $\hat{A}$ . All of the obstacles lie in the high dimensionality of augmentation distribution. Fortunately, though we can not accurately compute the value, it is efficient to sample from this distribution, *i.e.*, by performing augmentation on the natural data. Being aware of this, CPCL uses two practical losses to simulate the PCA process in an efficient way by sampling. The first contrastive-like loss leads the encoder to learn principal components of  $\hat{A}$ , which can be efficiently optimized by sampling like traditional contrastive methods. The second loss simulates the projection process and performs on-the-fly projection of  $\hat{A}$  through the training trajectory, which solves the difficulty of high dimensional projection.

**Learning principal components.** CPCL learns the principal components by an efficient contrastive-like loss. Besides its projection functionality, these learned principal components can also serve as the embeddings that preserve a kind of posterior distribution similarity, as we will show later.

In the SVD view,  $U\Sigma$  serves as the PCA projection results for samples and  $V$  contains the principal components [34]. However, if changing our view,  $V\Sigma$  can be seen as the representation of each column. Since each column of  $\hat{A}$  encodes probability on augmented data given natural data,  $V\Sigma$  can serve as the embeddings for augmented data and also preserve certain augmentation relationships, as we will show in Theorem 4.2 later. To leverage the extrapolation power of encoders like deep neural networks, we choose to design a loss that can guide the parameterized encoder  $f_\theta$  to learned similar embeddings as PCA. We employ the low-rank approximation objective with matrix factorization, similar to HaoChen et al. [11]:

$$\min_{F \in \mathbb{R}^{L \times k}} \mathcal{L}_{mf} = \|\hat{A}^\top \hat{A} - FF^\top\|_F^2, \quad (4)$$

where  $F$  stores the embedding of augmented data as will show in Lemma 4.1. According to Eckart–Young–Mirsky theorem [35], by optimizing  $\mathcal{L}_{mf}$ , we can get the optimal  $\hat{F}$ , which has the form  $\tilde{V}\tilde{\Sigma}Q$ ,  $Q \in \mathbb{R}^{k \times k}$  is an orthonormal matrix.  $\tilde{\Sigma}$  and  $\tilde{V}$  contains the top- $k$  singular values and right singular vectors. Expanding Equation (4), we get Contrastive Principal Component Loss for Augmented data (CPCL-A):

**Lemma 4.1** (CPCL-A loss). *Let  $F_{\mathbf{x},:} = \sqrt{d_{\mathbf{x}}}f_\theta^\top(\mathbf{x})$ ,  $\forall \mathbf{x} \in \mathcal{X}$ . Minimizing  $\mathcal{L}_{mf}$  is equivalent to minimize the following objective:*

$$\begin{aligned} \mathcal{L}_{CPCL-A} = & -2\mathbb{E}_{\substack{\bar{\mathbf{x}} \sim p(\bar{\mathbf{x}}), \\ \mathbf{x}_i \sim p(\mathbf{x}_i|\bar{\mathbf{x}}), \\ \mathbf{x}_j \sim p(\mathbf{x}_j|\bar{\mathbf{x}})}} f_\theta(\mathbf{x}_i)^\top f_\theta(\mathbf{x}_j) \\ & + N\mathbb{E}_{\mathbf{x}_1 \sim p_A(\mathbf{x}_1), \mathbf{x}_2 \sim p_A(\mathbf{x}_2)} \left[ \left( f_\theta(\mathbf{x}_1)^\top f_\theta(\mathbf{x}_2) \right)^2 \right] \end{aligned} \quad (5)$$

The proof can be found in Appendix B. In CPCL-A, the first term is the common alignment loss for augmented data and the second term is a form of uniformity loss [36, 37]. Both the two terms can be estimated by Monte-Carlo sampling. CPCL-A is a kind of contrastive loss resembling Equation (1). But unlike most of the others, it has theoretical meanings. We note that the form of CPCL-A differs from spectral loss [11] by adding an amplifying constant  $N$  before the uniformity term. This term is similar to the noise strength in NCE [38] or the number of negative samples in InfoNCE [2]. It can be proved that the learned embeddings by CPCL-A preserve the posterior distribution distances between augmented data:

**Theorem 4.2** (Almost isometry for posterior distances). *Assume  $f_\theta$  is a universal encoder,  $\sigma_{k+1}$  is the  $(k+1)$ -th largest singular value of  $\hat{A}$ ,  $d_{\min} = \min_{\mathbf{x}} d_{\mathbf{x}}$ , and  $\delta_{\mathbf{x}_1\mathbf{x}_2} = \mathbb{I}(\mathbf{x}_1 = \mathbf{x}_2)$ , the minimizer  $\theta^*$  of*

$\mathcal{L}_{CPCL-A}$  satisfies:

$$d_{\text{post}}^2(\mathbf{x}_1, \mathbf{x}_2) - \frac{2\sigma_{k+1}^2}{d_{\text{min}}} (1 - \delta_{\mathbf{x}_1\mathbf{x}_2}) \leq \|f_{\theta^*}(\mathbf{x}_1) - f_{\theta^*}(\mathbf{x}_2)\|_2^2 \leq d_{\text{post}}^2(\mathbf{x}_1, \mathbf{x}_2), \quad \forall \mathbf{x}_1, \mathbf{x}_2 \in \mathcal{X}$$

where the posterior distance

$$d_{\text{post}}^2(\mathbf{x}_1, \mathbf{x}_2) = \sum_{\bar{\mathbf{x}} \in \bar{\mathcal{X}}} (p_{\mathcal{A}}(\bar{\mathbf{x}}|\mathbf{x}_1) - p_{\mathcal{A}}(\bar{\mathbf{x}}|\mathbf{x}_2))^2$$

measures the squared Euclidean distance between the posterior distribution  $p_{\mathcal{A}}(\bar{\mathbf{x}}|\mathbf{x}) = \frac{p(\mathbf{x}|\bar{\mathbf{x}})p(\bar{\mathbf{x}})}{p_{\mathcal{A}}(\mathbf{x})}$ .

We give the proof in Appendix C. Theorem 4.2 states that the optimal encoder for CPCL-A preserves the distance of posterior distributions between augmented data within an error related to embedding size  $k$ . As  $k$  increase to  $N$ , the error decrease to 0. It corresponds to the phenomenon that a larger embedding size leads to better contrastive performance [5]. The posterior distribution  $p_{\mathcal{A}}(\bar{\mathbf{x}}|\mathbf{x})$  represents the probability that a given augmented sample  $\mathbf{x}$  is created by a natural sample  $\bar{\mathbf{x}}$ . Augmented data that are only produced by the same natural sample will have the smallest distance, and embeddings of those in overlapped areas will be pulled together by CPCL-A. Since the overlapped area are usually created by two same-class samples, CPCL-A can form semantically meaningful embedding space.

It is also noticeable that the optimal encoder meets the similarity preserving condition (Equation (2)) but concerning the posterior distribution for augmented data not the augmentation distribution for natural data. Since what we really care about is the distribution of natural data, we further propose a projection loss that helps learn good embeddings for all the natural data.

**On-the-fly Projection.** As is stated in the previous part, the learned embeddings by CPCL-A not only serve as certain embeddings for augmented data but also contain principal components of normalized augmentation feature. Based on this, we propose to use these embeddings to act as a projection operator to ensure meaningful embeddings for all the natural data. To be specific, denote the embedding matrix for all augmented data as  $F^{\text{aug}} (\in \mathbb{R}^{L \times k})$ , where each row  $F_{\mathbf{x},:}^{\text{aug}} = f_{\theta^*}(\mathbf{x})$ . From Equation (4) and  $\hat{F}_{\mathbf{x},:} = \sqrt{d_{\mathbf{x}}} f_{\theta^*}^{\top}(\mathbf{x})$ , it can be easily seen that:

$$F^{\text{aug}} = D^{-\frac{1}{2}} \hat{F} = D^{-\frac{1}{2}} \tilde{V} \tilde{\Sigma} Q$$

Similar to PCA [14] that project the original feature by  $V$ , the principal components, we propose to use  $F^{\text{aug}}$  to project the augmentation feature to get the embeddings for each natural sample. Denote the embedding matrix for natural data as  $F^{\text{nat}} (\in \mathbb{R}^{N \times k})$ , where each row  $F_{\bar{\mathbf{x}},:}^{\text{nat}}$  represents the embeddings of  $\bar{\mathbf{x}}$ . We compute  $F^{\text{nat}}$  as follows:

$$F^{\text{nat}} = A F^{\text{aug}} = \hat{A} D^{\frac{1}{2}} D^{-\frac{1}{2}} \tilde{V} \tilde{\Sigma} Q = (\tilde{U} \tilde{\Sigma}) \tilde{\Sigma} Q, \quad (6)$$

where  $\tilde{\Sigma}, \tilde{U}$  contain the top- $k$  singular values and corresponding left singular vectors. It is noticeable that  $F^{\text{nat}}$  is exactly the PCA projection result multiplied by an additional matrix  $\tilde{\Sigma} Q$ . Fortunately, such additional linear transformation does not affect the linear probe performance [11]. With Equation (6), the embedding of each natural sample can be computed as follows:

$$F_{\bar{\mathbf{x}},:}^{\text{nat}} = A_{\bar{\mathbf{x}},:} F^{\text{aug}} = \sum_{\mathbf{x}} p(\mathbf{x}|\bar{\mathbf{x}}) f_{\theta^*}^{\top}(\mathbf{x}) = \mathbb{E}_{\mathbf{x} \sim p(\mathbf{x}|\bar{\mathbf{x}})} f_{\theta^*}^{\top}(\mathbf{x}) \quad (7)$$

which is exactly the expected feature over the augmentation distribution. Similar to Theorem 4.2, the embeddings calculated by Equation (7) also present a certain isometry property for the augmentation distribution distances:

**Theorem 4.3** (Almost isometry for weighted augmentation distances). *Assume  $f_{\theta}$  is a universal encoder,  $\sigma_{k+1}$  is the  $(k+1)$ -th largest singular value of  $\hat{A}$ ,  $\delta_{\bar{\mathbf{x}}_1\bar{\mathbf{x}}_2} = \mathbb{I}(\bar{\mathbf{x}}_1 = \bar{\mathbf{x}}_2)$ , let the minimizer of  $\mathcal{L}_{CPCL-A}$  be  $\theta^*$  and  $g(\bar{\mathbf{x}}) = \mathbb{E}_{\mathbf{x} \sim p(\mathbf{x}|\bar{\mathbf{x}})} f_{\theta^*}(\mathbf{x})$  as in Equation (7), then:*

$$d_{\text{w-aug}}^2(\bar{\mathbf{x}}_1, \bar{\mathbf{x}}_2) - 2\sigma_{k+1}^2 (1 - \delta_{\bar{\mathbf{x}}_1\bar{\mathbf{x}}_2}) \leq \|g(\bar{\mathbf{x}}_1) - g(\bar{\mathbf{x}}_2)\|_{\Sigma_k^{-2}}^2 \leq d_{\text{w-aug}}^2(\bar{\mathbf{x}}_1, \bar{\mathbf{x}}_2), \quad \forall \bar{\mathbf{x}}_1, \bar{\mathbf{x}}_2 \in \bar{\mathcal{X}}$$

where  $\|\cdot\|_{\Sigma_k^{-2}}$  represent the Mahalanobis distance with matrix  $\Sigma_k^{-2}, \Sigma_k = \text{diag}([\sigma_1, \sigma_2, \dots, \sigma_k])$  is the diagonal matrix containing top- $k$  sigular values and the weighted augmentation distance

$$d_{w\text{-aug}}^2(\bar{\mathbf{x}}_1, \bar{\mathbf{x}}_2) = \frac{1}{N} \sum_{\mathbf{x} \in \mathcal{X}} \frac{(p(\mathbf{x}|\bar{\mathbf{x}}_1) - p(\mathbf{x}|\bar{\mathbf{x}}_2))^2}{p_{\mathcal{A}}(\mathbf{x})}$$

measures the weighted squared Euclidean distance between the augmentation distribution  $p(\mathbf{x}|\bar{\mathbf{x}})$ .

Different from Theorem 4.2, which presents isometry between Euclidean distances in embeddings and augmentation distribution, Theorem 4.3 presents isometry between Mahalanobis distances. The weighted augmentation distances weight the Euclidean distances by  $p_{\mathcal{A}}(\mathbf{x})$  which serves the same functionality as  $d_{\mathbf{x}}$ .  $d_{w\text{-aug}}$  can be regarded as a valid augmentation distance measure  $d_{\mathcal{A}}$  as in Equation (2) and  $F^{\text{nat}}$  preserve such distance. However, as is stated before, the additional projection process is not efficient, *i.e.*, we need exponentially many samples from  $p(\mathbf{x}|\bar{\mathbf{x}})$ . We notice that samples during training CPCL-A can be reused. For this reason, we propose an on-the-fly projection loss that directly use the current encoder for projection:

$$\mathcal{L}_{\text{proj}} = \mathbb{E}_{\bar{\mathbf{x}} \sim p(\bar{\mathbf{x}})} [\|f_{\theta}(\bar{\mathbf{x}}) - \mathbb{E}_{p(\mathbf{x}|\bar{\mathbf{x}})} f_{\theta}(\mathbf{x})\|_2^2] \quad (8)$$

**Full objective of CPCL.** Based on the discussion of the above parts, CPCL simultaneously learns the principal components by CPCL-A and projects natural data by an on-the-fly projection loss. The full objective of CPCL has the following form:

$$\mathcal{L}_{\text{CPCL-Full}} = \mathcal{L}_{\text{CPCL-A}} + \alpha \mathcal{L}_{\text{proj}} \quad (9)$$

where  $\alpha$  is a trade-off hyperparameter. In practice, we find the constant  $N$  lead to numerical instability. So we turn the  $N$  into a tunable noise strength  $K$ . We describe the empirical loss in Appendix A, but the algorithm is summarized here in Algorithm 1 for clarification.

---

#### Algorithm 1 Contrastive Principal Component Learning Algorithm

---

**Require:** Unlabeled natural dataset  $\{\mathbf{x}_i\}_{i=1}^N$ ; Augmentation function  $\mathcal{A}$ ; Encoding model  $f_{\theta}$  parameterized with  $\theta$ ; projection paramter  $\alpha$ ; Noise Stregth  $K$ ; Batch size  $B$ .

- 1: **for** sampled minibatch  $\{\mathbf{x}_i\}_{i=1}^B$  **do**
  - 2:   **for**  $i = 1, 2, \dots, B$  **do**
  - 3:      $\mathbf{x}_i^{(1)} = \mathcal{A}(\bar{\mathbf{x}}_i), \mathbf{x}_i^{(2)} = \mathcal{A}(\bar{\mathbf{x}}_i)$
  - 4:   **end for**
  - 5:    $\mathcal{L}_{\text{CPCL-Full}} = -\frac{2}{B} \sum_{i=1}^B f_{\theta}^{\top}(\mathbf{x}_i^{(1)}) f_{\theta}(\mathbf{x}_i^{(2)}) + \frac{K}{B(B-1)} \sum_{i \neq j} (f_{\theta}^{\top}(\mathbf{x}_i^{(1)}) f_{\theta}(\mathbf{x}_j^{(2)}))^2 + \alpha \|f_{\theta}(\bar{\mathbf{x}}) - \frac{f_{\theta}(\mathbf{x}_i^{(1)}) + f_{\theta}(\mathbf{x}_i^{(2)})}{2}\|_2^2$
  - 6:   update  $\theta$  with w.r.t  $\mathcal{L}_{\text{CPCL-Full}}$ .
  - 7: **end for**
  - 8: **return**  $f_{\theta}$
- 

## 5 Synthetic Example

In this section, we experiment with our contrastive principal component learning method on a synthetic mixture component data with a Gaussian augmentation method. In this example, we aim to show the relationship between semantic similarity and posterior/weighted augmentation distances. We also show the effectiveness of our method compared to traditional contrastive learning. In this example, the natural data  $\bar{\mathbf{x}}$  are sampled from a mixture gaussian with  $c$  component:

$$p(\bar{\mathbf{x}}) = \sum_{i=1}^c \pi_i \mathcal{N}(\boldsymbol{\mu}_i, s_i I)$$

We use Gaussian noise as the data augmentation of a natural data sample, *i.e.*,  $\mathcal{A}(\bar{\mathbf{x}}) = \bar{\mathbf{x}} + \xi$  where  $\xi \sim \mathcal{N}(0, s_a I)$ . Concretely, we conduct our experiment on 2-D data with  $c = 4, \pi_i = \frac{1}{c}, s_i = 1$  and the

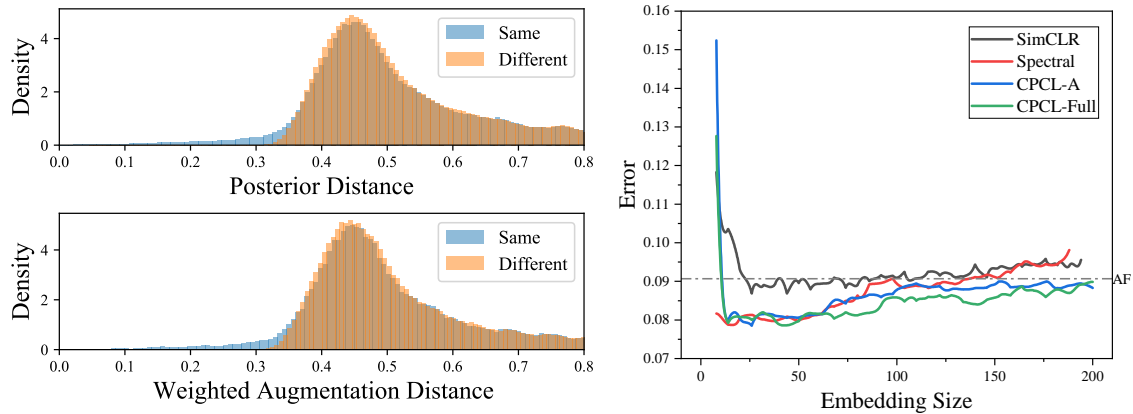


Figure 3: Synthetic experiments on mixture Gaussian data with Gaussian noise as augmentation. (a) The posterior distance and weighted augmentation distances among data that is sampled from the same component and different components. It reveals the correlation between semantic similarity and the two distances, especially when the distance is small. (b) Comparison of linear classification performance among SimCLR, Spectral and our methods with various embedding dimensions ranging from 4 to 200. The dashed line represents the result when directly using *Augmentation Feature* (AF). CPCL-A outperforms SimCLR and Spectral. CPCL-Full further improves.

$\mu_i$  uniformly distributed on a circle with radius 2. For each component, we sample 200 natural data with the index of the component as their label. For each natural datum, we augment it for 2 times with  $s_a = 4$ , which results in totally 1600 augmented data. We compute the augmentation probability for between  $x$  and  $\bar{x}$  by  $p(x|\bar{x})$  and we normalize the probability by for each  $\bar{x}$ .

First, we plot the distribution of posterior distances for pairs of augmented data and weighted augmentation distances for pairs of natural data in Figure 3 left. The two distances appear similar distribution because the synthetic data are Gaussian. It can be seen that data from the same component tend to have small distances, while from different components, their distances are large. In low distance areas, there are same-class pairs, meaning that the two distances are reliable metrics for judging the semantic similarity. In all, this picture reveals the correlation between semantic similarity and posterior/weighted augmentation distances.

Second, we compare our methods with SimCLR [5], the traditional contrastive method and Spectral [11], which similarly learns embeddings with spectral theory. We test the learned embeddings using a Logistic Regression classifier and report the error rate of the prediction in Figure 3 right. We also report performance when directly using *augmentation feature* (AF). First, AF has the discriminability for simple linear classifiers. As the embedding size increase, SimCLR and Spectral tend to underperform AF, while our methods consistently outperform. It may be confusing since our method performs dimension reduction on this feature. But we note that as the embedding size increase, the complexity of the linear model also increases, which affect the generalizability. All of the methods in Figure 3 right show degradation of this kind. However, our methods consistently outperform others, which shows the superiority of CPCL. Also, by adding projection loss, CPCL-Full improves CPCL-A by a margin. Additionally, traditional contrastive learning like SimCLR achieves similar performance as our methods. We think it reveals that traditional contrastive learning has the same functionality as our methods.

## 6 Experiments

### 6.1 Setup and Implementation

**Dataset.** In this paper, we conduct experiments mainly on the following datasets with RTX-3090  $\times$  4. **CIFAR-10** and **CIFAR-100** [39]: two dataset containing totally 500K images of size  $32 \times 32$  from 10 and 100 classes respectively. **STL-10** [40]: derived from ImageNet [41], with  $96 \times 96$  resolution images with 5K labeled training data from 10 classes. Additionally 100K unlabeled images are used for unsupervised



Table 1: Top-1 linear classification accuracy and 5-NN accuracy on four different datasets with a ResNet-18 encoder. We use **bold** to mark the best results and underline to mark the second best results. (repro.) means the results are reproduced by our code.

method	CIFAR-10		CIFAR-100		STL-10		Tiny ImageNet	
	Linear	5-NN	Linear	5-NN	Train	5-NN	Linear	5-NN
SimCLR [5] (repro.)	90.88	88.25	65.53	<u>55.32</u>	89.27	<u>85.44</u>	<u>46.16</u>	<b>31.43</b>
BYOL [27] (repro.)	<u>91.20</u>	<u>89.52</u>	64.85	54.92	88.64	85.07	44.35	29.66
SimSiam [28] (repro.)	91.06	89.43	65.41	54.84	<b>90.08</b>	<b>85.48</b>	45.17	30.41
Spectral [11] (repro.)	90.28	87.25	65.42	55.05	89.16	84.23	45.69	29.32
CPCL-A (ours)	90.35	87.38	<u>65.69</u>	54.57	88.47	84.41	46.08	30.97
CPCL-Full (ours)	<b>91.58</b>	<b>89.79</b>	<b>66.09</b>	<b>55.59</b>	<u>89.88</u>	85.20	<b>46.41</b>	<u>31.39</u>

learning. **Tiny ImageNet**: a reduced version of ImageNet [41], composed of 100K images scaled down to  $64 \times 64$  from 200 classes. **ImageNet-100** [3]: a subset of ImageNet, with 100-classes. **ImageNet** [41], the large-scale dataset with 1K classes.

**Network Structure.** Following common practice [5, 42, 6], we use the encoder-projector structure during training, where the projector projects the embeddings into a low dimensional space. For CIFAR-10 and CIFAR-100, we use the CIFAR variant of ResNet-18 [43, 28] as the encoder. We use a two-layer MLP as the projector whose hidden dimension is half of the input dimension and output dimension is 64. For STL-10 and Tiny ImageNet, only the max-pooling layer is disabled following [28, 44]. For these two datasets, we use the same projector structure except for the output dimension is 128. For ImageNet, we use ResNet-50 with the same projector as Chen et al. [5].

**Image Transformation.** Following the common practice of contrastive learning [5], we apply the following augmentations sequentially during training: (a) crops with a random size; (b) random horizontal flipping; (c) color jittering; (d) grayscaling. For ImageNet-100 and ImageNet, we use the same implementation as [5].

**Optimizer and other Hyper-parameters.** For datasets except ImageNet, adam optimizer [45] is used for all the datasets. For CIFAR-10 and CIFAR-100, we use 800 epochs with a learning rate  $3 \times 10^{-3}$ . For Tiny ImageNet and STL-10, we train 1,000 epochs with learning rate  $2 \times 10^{-3}$ . We use a learning rate warm-up for the first 500 iterations of the optimizer, and a 0.1 learning rate decay at 100, 50, 20 epochs before the end. Due to hardware resource restrictions, we use a mini-batch of size 512. The weight decay is  $1 \times 10^{-6}$  if not specified. Following common practice in contrastive learning, we normalize the projected feature into a sphere. For CIFAR-10, we use  $\alpha = 1$ . For the rest datasets, we use  $\alpha = 0.2$ . By default,  $K$  is set to 2. For ImageNet, we use the same hyperparameters as [5] except batch size being 256,  $\alpha = 0.2$  and  $K = 2$ .

**Evaluation Protocol.** We evaluate the learned representation on two most commonly used protocols – linear classification [15, 46] and k-nearest neighbors classifier [28]. In all the experiments, we train the linear classifier for 100 epochs. The learning rate is exponentially decayed from  $10^{-2}$  to  $10^{-6}$ . The weight decay is  $1 \times 10^{-6}$ . We report the classification accuracy on test embeddings as well as the accuracy of a 5-Nearest Neighbors classifier for datasets except for ImageNet.

## 6.2 Performance Comparison with state-of-the-art

In Table 1, we compare our method on various small-scale or mid-scale benchmarks with several state-of-the-art methods including SimCLR [5], BYOL [27], SimSiam [28] and Spectral [11]. SimCLR uses is a method that uses contrastive loss. BYOL and SimSiam do not use negative samples. Spectral is a similar loss derived from the idea of spectral clustering. From Table 1, we can see that our CPCL-Full method achieves competitive results on small-scale or mid-scale benchmarks, achieving either the best or the

Table 2: Left: Top-1 classification accuracy and 5-NN accuracy on ImageNet-100 with ResNet-18. †: results are taken from [44]. \*: results are taken from [29].(repro.) means the results are reproduced by our code. Right: Top-1 classification accuracy on ImageNet with ResNet-50, results are taken from [28, 11]. We use **bold** to mark the best results and underline to mark the second best results.

ImageNet-100	Linear	5-NN	ImageNet	100 epochs
MoCo† [47]	72.80	-	SimCLR [5]	66.5
$\mathcal{L}_{align} + \mathcal{L}_{uniform}$ † [36]	74.60	-	MoCo v2 [6]	67.4
W-MSE 2† [44]	<u>76.00</u>	<b>67.04</b>	BYOL [27]	66.5
InfoMin* [29]	74.90	-	SwAV [48]	66.5
SimCLR [5] (repro.)	75.62	62.70	SimSiam [28]	<u>68.1</u>
Spectral [11] (repro.)	75.52	61.80	Spectral [11]	66.97
CPCL-A (ours)	75.80	62.54	CPCL-A (ours)	67.21
CPCL-Full (ours)	<b>76.02</b>	<u>63.20</u>	CPCL-Full (ours)	<b>68.32</b>

second-best results on all the benchmarks except the 5-NN evaluation on STL-10. Also, CPCL-A differs from CPCL-Full in the projection loss. In all the benchmarks, we can see the projection loss improves performance, in accordance with our synthetic experiment.

For large-scale benchmarks, we compare several methods on ImageNet-100 and ImageNet. On ImageNet-100, we compare our method additionally to MoCo [47],  $\mathcal{L}_{align} + \mathcal{L}_{uniform}$  [36], W-MSE 2 [44] and InfoMin [29]. Note that except W-MSE, results of the other three methods are reported when using the ResNet-50 encoder, which has more capacity than ResNet18. Our method can also achieve state-of-the-art results among them. This means our method is also effective with relatively small encoders even on large-scale datasets. On ImageNet, we see that CPCL-A achieves competitive performance against state-of-the-art contrastive methods [5, 6, 27, 48, 28, 11] and CPCL-Full achieves the best.

## 7 Conclusion

In this paper, we provide a new way of constructing self-supervised contrastive learning tasks by modeling similarity through augmentation overlap, which is motivated by the observation that semantically similar data usually creates similar augmentations. We propose contrastive principal component learning to perform PCA on augmentation feature efficiently. Interestingly, our methods have a similar form as the traditional contrastive loss and may explain the ability of contrastive loss. We hope our paper can inspire more thoughts about how to measure similarity in self-supervised learning and how to construct contrastive learning tasks. Currently, we limit our work to discrete augmentation distribution and we put investigation of continuous distribution for future work.

## References

- [1] Zhirong Wu, Yuanjun Xiong, Stella X Yu, and Dahua Lin. Unsupervised feature learning via non-parametric instance discrimination. In *CVPR*, pages 3733–3742, 2018.
- [2] Aäron van den Oord, Yazhe Li, and Oriol Vinyals. Representation learning with contrastive predictive coding. *CoRR*, abs/1807.03748, 2018.
- [3] Yonglong Tian, Dilip Krishnan, and Phillip Isola. Contrastive multiview coding. In *ECCV*, pages 776–794, 2020.
- [4] Kaiming He, Haoqi Fan, Yuxin Wu, Saining Xie, and Ross Girshick. Momentum contrast for unsupervised visual representation learning. In *CVPR*, pages 9729–9738, 2020.
- [5] Ting Chen, Simon Kornblith, Mohammad Norouzi, and Geoffrey E. Hinton. A simple framework for contrastive learning of visual representations. In *ICML*, pages 1597–1607, 2020.
- [6] Xinlei Chen, Haoqi Fan, Ross B. Girshick, and Kaiming He. Improved baselines with momentum contrastive learning. *CoRR*, abs/2003.04297, 2020.

- [7] Ishan Misra and Laurens van der Maaten. Self-supervised learning of pretext-invariant representations. In *CVPR*, pages 6707–6717, 2020.
- [8] Ching-Yao Chuang, Joshua Robinson, Yen-Chen Lin, Antonio Torralba, and Stefanie Jegelka. Debaised contrastive learning. In *NeurIPS*, 2020.
- [9] Nikunj Saunshi, Orestis Plevrakis, Sanjeev Arora, Mikhail Khodak, and Hrishikesh Khandeparkar. A theoretical analysis of contrastive unsupervised representation learning. In *ICML*, pages 5628–5637, 2019.
- [10] Christopher Tosh, Akshay Krishnamurthy, and Daniel Hsu. Contrastive learning, multi-view redundancy, and linear models. In *Algorithmic Learning Theory*, pages 1179–1206, 2021.
- [11] Jeff Z. HaoChen, Colin Wei, Adrien Gaidon, and Tengyu Ma. Provable guarantees for self-supervised deep learning with spectral contrastive loss. In *NeurIPS*, pages 5000–5011, 2021.
- [12] Yifei Wang, Qi Zhang, Yisen Wang, Jiansheng Yang, and Zhouchen Lin. Chaos is a ladder: A new theoretical understanding of contrastive learning via augmentation overlap. *CoRR*, abs/2203.13457, 2022.
- [13] Barbara Zitova and Jan Flusser. Image registration methods: a survey. *Image and vision computing*, 21(11):977–1000, 2003.
- [14] Harold Hotelling. Analysis of a complex of statistical variables into principal components. *Journal of educational psychology*, 24(6):417, 1933.
- [15] Richard Zhang, Phillip Isola, and Alexei A. Efros. Colorful image colorization. In *ECCV*, pages 649–666, 2016.
- [16] Deepak Pathak, Philipp Krahenbuhl, Jeff Donahue, Trevor Darrell, and Alexei A Efros. Context encoders: Feature learning by inpainting. In *CVPR*, pages 2536–2544, 2016.
- [17] Carl Doersch, Abhinav Gupta, and Alexei A Efros. Unsupervised visual representation learning by context prediction. In *ICCV*, pages 1422–1430, 2015.
- [18] Mehdi Noroozi and Paolo Favaro. Unsupervised learning of visual representations by solving jigsaw puzzles. In *ECCV*, pages 69–84. Springer, 2016.
- [19] Spyros Gidaris, Praveer Singh, and Nikos Komodakis. Unsupervised representation learning by predicting image rotations. 2018.
- [20] Ian J. Goodfellow, Jean Pouget-Abadie, Mehdi Mirza, Bing Xu, David Warde-Farley, Sherjil Ozair, Aaron C. Courville, and Yoshua Bengio. Generative adversarial nets. In *NIPS*, pages 2672–2680, 2014.
- [21] Diederik P. Kingma and Max Welling. Auto-encoding variational bayes. In *ICLR*, 2014.
- [22] Jeff Donahue and Karen Simonyan. Large scale adversarial representation learning. In *NeurIPS*, pages 10541–10551, 2019.
- [23] Tomás Mikolov, Ilya Sutskever, Kai Chen, Gregory S. Corrado, and Jeffrey Dean. Distributed representations of words and phrases and their compositionality. In *NIPS*, pages 3111–3119, 2013.
- [24] Jacob Devlin, Ming-Wei Chang, Kenton Lee, and Kristina Toutanova. BERT: pre-training of deep bidirectional transformers for language understanding. In *NAACL-HLT*, pages 4171–4186, 2019.
- [25] Philip Bachman, R. Devon Hjelm, and William Buchwalter. Learning representations by maximizing mutual information across views. In *NeurIPS*, pages 15509–15519, 2019.
- [26] Junnan Li, Pan Zhou, Caiming Xiong, and Steven C. H. Hoi. Prototypical contrastive learning of unsupervised representations. In *ICLR*, 2021.
- [27] Jean-Bastien Grill, Florian Strub, Florent Altché, Corentin Tallec, Pierre H. Richemond, Elena Buchatskaya, Carl Doersch, Bernardo Ávila Pires, Zhaohan Guo, Mohammad Gheshlaghi Azar, Bilal Piot, Koray Kavukcuoglu, Rémi Munos, and Michal Valko. Bootstrap your own latent - A new approach to self-supervised learning. In *NeurIPS*, 2020.

- [28] Xinlei Chen and Kaiming He. Exploring simple siamese representation learning. In *CVPR*, pages 15750–15758, 2021.
- [29] Yonglong Tian, Chen Sun, Ben Poole, Dilip Krishnan, Cordelia Schmid, and Phillip Isola. What makes for good views for contrastive learning? In *NeurIPS*, 2020.
- [30] Tete Xiao, Xiaolong Wang, Alexei A. Efros, and Trevor Darrell. What should not be contrastive in contrastive learning. In *ICLR*, 2021.
- [31] Nanxuan Zhao, Zhirong Wu, Rynson W. H. Lau, and Stephen Lin. What makes instance discrimination good for transfer learning? In *ICLR*, 2021.
- [32] Jason D. Lee, Qi Lei, Nikunj Saunshi, and Jiacheng Zhuo. Predicting what you already know helps: Provable self-supervised learning. In *NeurIPS*, pages 309–323, 2021.
- [33] Richard A Reyment and KG Jvreskog. *Applied factor analysis in the natural sciences*. Cambridge University Press, 1996.
- [34] Ian T Jolliffe. *Principal component analysis for special types of data*. Springer, 2002.
- [35] Carl Eckart and Gale Young. The approximation of one matrix by another of lower rank. *Psychometrika*, 1(3):211–218, 1936.
- [36] Tongzhou Wang and Phillip Isola. Understanding contrastive representation learning through alignment and uniformity on the hypersphere. In *ICML*, pages 9929–9939, 2020.
- [37] Ting Chen, Calvin Luo, and Lala Li. Intriguing properties of contrastive losses. In *NeurIPS*, pages 11834–11845, 2021.
- [38] Michael Gutmann and Aapo Hyvärinen. Noise-contrastive estimation: A new estimation principle for unnormalized statistical models. In *AISTATS*, pages 297–304, 2010.
- [39] Alex Krizhevsky, Geoffrey Hinton, et al. Learning multiple layers of features from tiny images. 2009.
- [40] Adam Coates, Andrew Y. Ng, and Honglak Lee. An analysis of single-layer networks in unsupervised feature learning. In *AISTATS*, pages 215–223, 2011.
- [41] Jia Deng, Wei Dong, Richard Socher, Li-Jia Li, Kai Li, and Li Fei-Fei. Imagenet: A large-scale hierarchical image database. In *CVPR*, pages 248–255, 2009.
- [42] Ting Chen, Simon Kornblith, Kevin Swersky, Mohammad Norouzi, and Geoffrey E. Hinton. Big self-supervised models are strong semi-supervised learners. In *NeurIPS*, 2020.
- [43] Kaiming He, Xiangyu Zhang, Shaoqing Ren, and Jian Sun. Deep residual learning for image recognition. In *CVPR*, pages 770–778, 2016.
- [44] Aleksandr Ermolov, Aliaksandr Siarohin, Enver Sangineto, and Nicu Sebe. Whitening for self-supervised representation learning. In *ICML*, pages 3015–3024, 2021.
- [45] Diederik P. Kingma and Jimmy Ba. Adam: A method for stochastic optimization. In *ICLR*, 2015.
- [46] Alexander Kolesnikov, Xiaohua Zhai, and Lucas Beyer. Revisiting self-supervised visual representation learning. In *CVPR*, pages 1920–1929, 2019.
- [47] Kaiming He, Haoqi Fan, Yuxin Wu, Saining Xie, and Ross B. Girshick. Momentum contrast for unsupervised visual representation learning. In *CVPR*, pages 9726–9735, 2020.
- [48] Mathilde Caron, Ishan Misra, Julien Mairal, Priya Goyal, Piotr Bojanowski, and Armand Joulin. Unsupervised learning of visual features by contrasting cluster assignments. In *NeurIPS*, 2020.

## A The Empirical Loss

$\mathcal{L}_{\text{CPCL-A}}$  consists of two parts, for the first part, *i.e.*, the alignment loss:

$$\begin{aligned} & \mathbb{E}_{\bar{\mathbf{x}} \sim p(\bar{\mathbf{x}}), \mathbf{x}_i \sim p(\mathbf{x}_i | \bar{\mathbf{x}}), \mathbf{x}_j \sim p(\mathbf{x}_j | \bar{\mathbf{x}})} f_{\theta}(\mathbf{x}_i)^{\top} f_{\theta}(\mathbf{x}_j) \\ &= \mathbb{E}_{\bar{\mathbf{x}} \sim p(\bar{\mathbf{x}})} \mathbb{E}_{\mathbf{x}_i \sim p(\mathbf{x}_i | \bar{\mathbf{x}})} \mathbb{E}_{\mathbf{x}_j \sim p(\mathbf{x}_j | \bar{\mathbf{x}})} f_{\theta}(\mathbf{x}_i)^{\top} f_{\theta}(\mathbf{x}_j) \end{aligned}$$

we use the mini-batch of natural sample to estimate  $\mathbb{E}_{\bar{\mathbf{x}} \sim p(\bar{\mathbf{x}})}$ . And we just use one sample to estimate  $\mathbb{E}_{\mathbf{x}_i \sim p(\mathbf{x}_i | \bar{\mathbf{x}})}$  and  $\mathbb{E}_{\mathbf{x}_j \sim p(\mathbf{x}_j | \bar{\mathbf{x}})}$  respectively. This leads to the traditional contrastive learning procedure : sample a mini-batch of natural data, augment it twice, compute the similarity of two augmented data.

For the second part,

$$\mathbb{E}_{\mathbf{x}_1 \sim p_{\mathcal{A}}(\mathbf{x}_1), \mathbf{x}_2 \sim p_{\mathcal{A}}(\mathbf{x}_2)} \left[ \left( f_{\theta}(\mathbf{x}_1)^{\top} f_{\theta}(\mathbf{x}_2) \right)^2 \right]$$

we use the in-batch augmented data to estimate  $\mathbb{E}_{\mathbf{x}_1 \sim p_{\mathcal{A}}(\mathbf{x}_1)}$ . Following common practice [5], we use two augmented data that are created by augmenting two different natural data to compute this term.

For  $\mathcal{L}_{\text{proj}}$ , it is not efficient to fully sample from  $p(\mathbf{x} | \bar{\mathbf{x}})$ . However, it is notable that:

$$\mathbb{E}_{\bar{\mathbf{x}} \sim p(\bar{\mathbf{x}})} \left[ \|f_{\theta}(\bar{\mathbf{x}}) - \mathbb{E}_{p(\mathbf{x} | \bar{\mathbf{x}})} f_{\theta}(\mathbf{x})\|_2^2 \right] = \mathbb{E}_{\bar{\mathbf{x}} \sim p(\bar{\mathbf{x}}), \mathbf{x}_i \sim p(\mathbf{x}_i | \bar{\mathbf{x}}), \mathbf{x}_j \sim p(\mathbf{x}_j | \bar{\mathbf{x}})} \left[ \left\| f_{\theta}(\bar{\mathbf{x}}) - \frac{f_{\theta}(\mathbf{x}_i) + f_{\theta}(\mathbf{x}_j)}{2} \right\|_2^2 \right]$$

so we can use the same strategy as  $\mathcal{L}_{\text{CPCL-A}}$  and reuse the samples.

In all, the algorithm is summarized in Algorithm 1 in Section 4.2.

## B Proof of Lemma 4.1

For convenient, we define  $M := \hat{A}^{\top} \hat{A}$ . The elements of  $M$  is:

$$M_{\mathbf{x}_1 \mathbf{x}_2} = \sum_{\bar{\mathbf{x}} \in \bar{\mathcal{X}}} \frac{p(\mathbf{x}_1 | \bar{\mathbf{x}}) p(\mathbf{x}_2 | \bar{\mathbf{x}})}{\sqrt{d_{\mathbf{x}_1}} \sqrt{d_{\mathbf{x}_2}}}, \mathbf{x}_1, \mathbf{x}_2 \in \mathcal{X} \quad (10)$$

Expanding Equation (4), we get:

$$\begin{aligned} \mathcal{L}_{mf} &= \sum_{\mathbf{x}_1, \mathbf{x}_2 \in \mathcal{X}} (M_{\mathbf{x}_1 \mathbf{x}_2} - F_{\mathbf{x}_1}^{\top} F_{\mathbf{x}_2})^2 \\ &= \sum_{\mathbf{x}_1, \mathbf{x}_2 \in \mathcal{X}} (M_{\mathbf{x}_1 \mathbf{x}_2} - \sqrt{d_{\mathbf{x}_1}} \sqrt{d_{\mathbf{x}_2}} f_{\theta}(\mathbf{x}_1)^{\top} f_{\theta}(\mathbf{x}_2))^2 \\ &= \text{const} - 2 \sum_{\mathbf{x}_1, \mathbf{x}_2 \in \mathcal{X}} \sqrt{d_{\mathbf{x}_1}} \sqrt{d_{\mathbf{x}_2}} M_{\mathbf{x}_1 \mathbf{x}_2} f_{\theta}(\mathbf{x}_1)^{\top} f_{\theta}(\mathbf{x}_2) + \sum_{\mathbf{x}_1, \mathbf{x}_2 \in \mathcal{X}} d_{\mathbf{x}_1} d_{\mathbf{x}_2} (f_{\theta}(\mathbf{x}_1)^{\top} f_{\theta}(\mathbf{x}_2))^2 \\ &= \text{const} - 2 \sum_{\mathbf{x}_1, \mathbf{x}_2 \in \mathcal{X}} \sum_{\bar{\mathbf{x}} \in \bar{\mathcal{X}}} p(\mathbf{x}_1 | \bar{\mathbf{x}}) p(\mathbf{x}_2 | \bar{\mathbf{x}}) f_{\theta}(\mathbf{x}_1)^{\top} f_{\theta}(\mathbf{x}_2) + \sum_{\mathbf{x}_1, \mathbf{x}_2 \in \mathcal{X}} d_{\mathbf{x}_1} d_{\mathbf{x}_2} (f_{\theta}(\mathbf{x}_1)^{\top} f_{\theta}(\mathbf{x}_2))^2 \end{aligned}$$

multiply by  $p(\bar{\mathbf{x}}) = \frac{1}{N}$  and replace  $d_{\mathbf{x}}$  with  $\sum_{\bar{\mathbf{x}}} p(\mathbf{x} | \bar{\mathbf{x}}) = N p_{\mathcal{A}}(\mathbf{x})$ . The objective becomes:

$$\begin{aligned} \min_{\theta} & -2 \sum_{\mathbf{x}_1, \mathbf{x}_2 \in \mathcal{X}} \sum_{\bar{\mathbf{x}} \in \bar{\mathcal{X}}} p(\mathbf{x}_1 | \bar{\mathbf{x}}) p(\mathbf{x}_2 | \bar{\mathbf{x}}) p(\bar{\mathbf{x}}) f_{\theta}(\mathbf{x}_1)^{\top} f_{\theta}(\mathbf{x}_2) \\ & + N \sum_{\mathbf{x}_1, \mathbf{x}_2 \in \mathcal{X}} p_{\mathcal{A}}(\mathbf{x}_1) p_{\mathcal{A}}(\mathbf{x}_2) (f_{\theta}(\mathbf{x}_1)^{\top} f_{\theta}(\mathbf{x}_2))^2 \\ &= -2 \mathbb{E}_{\bar{\mathbf{x}} \sim p(\bar{\mathbf{x}}), \mathbf{x}_i \sim \mathcal{A}(\mathbf{x}_i | \bar{\mathbf{x}}), \mathbf{x}_j \sim \mathcal{A}(\mathbf{x}_j | \bar{\mathbf{x}})} \left[ f_{\theta}(\mathbf{x}_1)^{\top} f_{\theta}(\mathbf{x}_2) \right] \\ & + N \mathbb{E}_{\mathbf{x}_1 \sim p_{\mathcal{A}}(\mathbf{x}_1), \mathbf{x}_2 \sim p_{\mathcal{A}}(\mathbf{x}_2)} \left[ (f_{\theta}(\mathbf{x}_1)^{\top} f_{\theta}(\mathbf{x}_2))^2 \right] \\ &= \mathcal{L}_{\text{CPCL-A}} \end{aligned}$$

## C Proof of Theorem 4.2

As in Appendix B, we define  $M := \hat{A}^\top \hat{A}$ . By Eckart–Young–Mirsky theorem [35], the minimizer  $\hat{F}$  of  $\|M - FF^\top\|_F^2$ , must have the form  $\hat{V}\hat{\Sigma}Q$ , where  $\hat{V}, \hat{\Sigma}$  contain the top- $k$  singular values and corresponding right singular vectors of  $\hat{A}$ ,  $Q \in \mathbb{R}^{k \times k}$  is some orthonormal matrix with  $Q^\top Q = I$ . Since we let  $F_{\mathbf{x}} = \sqrt{d_{\mathbf{x}}}f_{\theta}(\mathbf{x})$ , then the minimizer  $\theta^*$  must satisfy

$$f_{\theta^*}(\mathbf{x}) = Q \frac{\hat{\sigma} \odot \hat{\mathbf{v}}(\mathbf{x})}{\sqrt{d_{\mathbf{x}}}} = Q \frac{[\sigma_1 v_1(\mathbf{x}), \sigma_2 v_2(\mathbf{x}), \dots, \sigma_k v_k(\mathbf{x})]^\top}{\sqrt{d_{\mathbf{x}}}}.$$

where  $\odot$  is the element-wise multiplication. For convenience, we use  $\sigma_i$  to denote  $i$ -th largest singular value,  $u_i(\bar{\mathbf{x}}), v_i(\mathbf{x})$  to denote the element of  $i$ -th left/right singular value corresponding to  $\bar{\mathbf{x}}/\mathbf{x}$ . When  $p(\bar{\mathbf{x}}) = \frac{1}{N}$ ,  $d_{\mathbf{x}} = Np_{\mathcal{A}}(\mathbf{x}) = \frac{p_{\mathcal{A}}(\mathbf{x})}{p(\bar{\mathbf{x}})}$ . Then the posterior distance:

$$\begin{aligned} d_{\text{post}}^2(\mathbf{x}_1, \mathbf{x}_2) &= \sum_{\bar{\mathbf{x}} \in \bar{\mathcal{X}}} (p_{\mathcal{A}}(\bar{\mathbf{x}}|\mathbf{x}_1) - p_{\mathcal{A}}(\bar{\mathbf{x}}|\mathbf{x}_2))^2 \\ &= \sum_{\bar{\mathbf{x}} \in \bar{\mathcal{X}}} \left( \frac{p(\mathbf{x}_1|\bar{\mathbf{x}})p(\bar{\mathbf{x}})}{p_{\mathcal{A}}(\mathbf{x}_1)} - \frac{p(\mathbf{x}_2|\bar{\mathbf{x}})p(\bar{\mathbf{x}})}{p_{\mathcal{A}}(\mathbf{x}_2)} \right)^2 \\ &= \sum_{\bar{\mathbf{x}} \in \bar{\mathcal{X}}} \left( \frac{p(\mathbf{x}_1|\bar{\mathbf{x}})}{d_{\mathbf{x}_1}} - \frac{p(\mathbf{x}_2|\bar{\mathbf{x}})}{d_{\mathbf{x}_2}} \right)^2 \\ &= \sum_{\bar{\mathbf{x}} \in \bar{\mathcal{X}}} \left( \frac{\hat{A}_{\bar{\mathbf{x}}\mathbf{x}_1}}{\sqrt{d_{\mathbf{x}_1}}} - \frac{\hat{A}_{\bar{\mathbf{x}}\mathbf{x}_2}}{\sqrt{d_{\mathbf{x}_2}}} \right)^2 \\ &= \sum_{\bar{\mathbf{x}} \in \bar{\mathcal{X}}} \left( \sum_{i=1}^N \frac{\sigma_i u_i(\bar{\mathbf{x}}) v_i(\mathbf{x}_1)}{\sqrt{d_{\mathbf{x}_1}}} - \frac{\sigma_i u_i(\bar{\mathbf{x}}) v_i(\mathbf{x}_2)}{\sqrt{d_{\mathbf{x}_2}}} \right)^2 \\ &= \sum_{\bar{\mathbf{x}} \in \bar{\mathcal{X}}} \left( \sum_{i=1}^N \sigma_i u_i(\bar{\mathbf{x}}) \left( \frac{v_i(\mathbf{x}_1)}{\sqrt{d_{\mathbf{x}_1}}} - \frac{v_i(\mathbf{x}_2)}{\sqrt{d_{\mathbf{x}_2}}} \right) \right)^2 \\ &= \sum_{\bar{\mathbf{x}} \in \bar{\mathcal{X}}} \sum_{i, i'} \sigma_i u_i(\bar{\mathbf{x}}) \sigma_{i'} u_{i'}(\bar{\mathbf{x}}) \left( \frac{v_i(\mathbf{x}_1)}{\sqrt{d_{\mathbf{x}_1}}} - \frac{v_i(\mathbf{x}_2)}{\sqrt{d_{\mathbf{x}_2}}} \right) \left( \frac{v_{i'}(\mathbf{x}_1)}{\sqrt{d_{\mathbf{x}_1}}} - \frac{v_{i'}(\mathbf{x}_2)}{\sqrt{d_{\mathbf{x}_2}}} \right) \\ &= \sum_{i, i'} \sigma_i \sigma_{i'} \left( \frac{v_i(\mathbf{x}_1)}{\sqrt{d_{\mathbf{x}_1}}} - \frac{v_i(\mathbf{x}_2)}{\sqrt{d_{\mathbf{x}_2}}} \right) \left( \frac{v_{i'}(\mathbf{x}_1)}{\sqrt{d_{\mathbf{x}_1}}} - \frac{v_{i'}(\mathbf{x}_2)}{\sqrt{d_{\mathbf{x}_2}}} \right) \sum_{\bar{\mathbf{x}} \in \bar{\mathcal{X}}} u_i(\bar{\mathbf{x}}) u_{i'}(\bar{\mathbf{x}}) \\ &\stackrel{(1)}{=} \sum_{i, i'} \sigma_i \sigma_{i'} \left( \frac{v_i(\mathbf{x}_1)}{\sqrt{d_{\mathbf{x}_1}}} - \frac{v_i(\mathbf{x}_2)}{\sqrt{d_{\mathbf{x}_2}}} \right) \left( \frac{v_{i'}(\mathbf{x}_1)}{\sqrt{d_{\mathbf{x}_1}}} - \frac{v_{i'}(\mathbf{x}_2)}{\sqrt{d_{\mathbf{x}_2}}} \right) \delta_{i, i'} \\ &= \sum_{i=1}^N \sigma_i^2 \left( \frac{v_i(\mathbf{x}_1)}{\sqrt{d_{\mathbf{x}_1}}} - \frac{v_i(\mathbf{x}_2)}{\sqrt{d_{\mathbf{x}_2}}} \right)^2 \end{aligned} \tag{11}$$

(1) is due to the orthogonality of singular vectors. Note that:

$$\begin{aligned}
& \sum_{i=1}^N \left( \frac{v_i(\mathbf{x}_1)}{\sqrt{d_{\mathbf{x}_1}}} - \frac{v_i(\mathbf{x}_2)}{\sqrt{d_{\mathbf{x}_2}}} \right)^2 \\
&= \sum_{i=1}^L \left( \frac{v_i(\mathbf{x}_1)}{\sqrt{d_{\mathbf{x}_1}}} - \frac{v_i(\mathbf{x}_2)}{\sqrt{d_{\mathbf{x}_2}}} \right)^2 - \sum_{i=N+1}^L \left( \frac{v_i(\mathbf{x}_1)}{\sqrt{d_{\mathbf{x}_1}}} - \frac{v_i(\mathbf{x}_2)}{\sqrt{d_{\mathbf{x}_2}}} \right)^2 \\
&\leq \sum_{i=1}^L \left( \frac{v_i(\mathbf{x}_1)}{\sqrt{d_{\mathbf{x}_1}}} - \frac{v_i(\mathbf{x}_2)}{\sqrt{d_{\mathbf{x}_2}}} \right)^2 \\
&= \sum_{i=1}^L \frac{v_i^2(\mathbf{x}_1)}{d_{\mathbf{x}_1}} + \sum_{i=1}^L \frac{v_i^2(\mathbf{x}_2)}{d_{\mathbf{x}_2}} - 2 \sum_{i=1}^L \frac{v_i(\mathbf{x}_1)v_i(\mathbf{x}_2)}{\sqrt{d_{\mathbf{x}_1}}\sqrt{d_{\mathbf{x}_2}}} \\
&= \frac{1}{d_{\mathbf{x}_1}} + \frac{1}{d_{\mathbf{x}_2}} - \frac{2\delta_{\mathbf{x}_1\mathbf{x}_2}}{\sqrt{d_{\mathbf{x}_1}}\sqrt{d_{\mathbf{x}_2}}} \\
&\stackrel{(2)}{\leq} \left( \frac{1}{d_{\mathbf{x}_1}} + \frac{1}{d_{\mathbf{x}_2}} \right) (1 - \delta_{\mathbf{x}_1\mathbf{x}_2}) \\
&\leq \frac{2}{d_{\min}} (1 - \delta_{\mathbf{x}_1\mathbf{x}_2})
\end{aligned}$$

(2) can be deduced by considering conditions whether  $\mathbf{x}_1 = \mathbf{x}_2$  or not. Then:

$$\begin{aligned}
& \|f_{\theta^*}(\mathbf{x}_1) - f_{\theta^*}(\mathbf{x}_2)\|^2 \\
&= \sum_{i=1}^k \sigma_i^2 \left( \frac{v_i(\mathbf{x}_1)}{\sqrt{d_{\mathbf{x}_1}}} - \frac{v_i(\mathbf{x}_2)}{\sqrt{d_{\mathbf{x}_2}}} \right)^2 \\
&= d_{\text{post}}^2(\mathbf{x}_1, \mathbf{x}_2) - \sum_{i=k}^N \sigma_i^2 \left( \frac{v_i(\mathbf{x}_1)}{\sqrt{d_{\mathbf{x}_1}}} - \frac{v_i(\mathbf{x}_2)}{\sqrt{d_{\mathbf{x}_2}}} \right)^2 \quad (\leq d_{\text{post}}^2(\mathbf{x}_1, \mathbf{x}_2)) \\
&\geq d_{\text{post}}^2(\mathbf{x}_1, \mathbf{x}_2) - \sigma_{k+1}^2 \sum_{i=k+1}^N \left( \frac{v_i(\mathbf{x}_1)}{\sqrt{d_{\mathbf{x}_1}}} - \frac{v_i(\mathbf{x}_2)}{\sqrt{d_{\mathbf{x}_2}}} \right)^2 \\
&\geq d_{\text{post}}^2(\mathbf{x}_1, \mathbf{x}_2) - \sigma_{k+1}^2 \sum_{i=1}^N \left( \frac{v_i(\mathbf{x}_1)}{\sqrt{d_{\mathbf{x}_1}}} - \frac{v_i(\mathbf{x}_2)}{\sqrt{d_{\mathbf{x}_2}}} \right)^2 \\
&\geq d_{\text{post}}^2(\mathbf{x}_1, \mathbf{x}_2) - \frac{2\sigma_{k+1}^2}{d_{\min}} (1 - \delta_{\mathbf{x}_1\mathbf{x}_2})
\end{aligned}$$

Therefore, we have proved Theorem 4.2.

## D Proof of Theorem 4.3

similar to Appendix C,

$$\begin{aligned}
d_{\text{w-aug}}^2(\bar{\mathbf{x}}_1, \bar{\mathbf{x}}_2) &= \sum_{\mathbf{x} \in \mathcal{X}} \frac{1}{Np_{\mathcal{A}}(\mathbf{x})} (p(\mathbf{x}|\bar{\mathbf{x}}_1) - p(\mathbf{x}|\bar{\mathbf{x}}_2))^2 \\
&= \sum_{\mathbf{x} \in \mathcal{X}} \left( \frac{p(\mathbf{x}|\bar{\mathbf{x}}_1)}{\sqrt{Np_{\mathcal{A}}(\mathbf{x})}} - \frac{p(\mathbf{x}|\bar{\mathbf{x}}_2)}{\sqrt{Np_{\mathcal{A}}(\mathbf{x})}} \right)^2 \\
&= \sum_{\mathbf{x} \in \mathcal{X}} \left( \frac{p(\mathbf{x}|\bar{\mathbf{x}}_1)}{\sqrt{d_{\mathbf{x}}}} - \frac{p(\mathbf{x}|\bar{\mathbf{x}}_2)}{\sqrt{d_{\mathbf{x}}}} \right)^2 \\
&= \sum_{\mathbf{x} \in \mathcal{X}} \left( \hat{A}_{\bar{\mathbf{x}}_1 \mathbf{x}} - \hat{A}_{\bar{\mathbf{x}}_2 \mathbf{x}} \right)^2 \\
&= \sum_{\mathbf{x} \in \mathcal{X}} \left( \sum_{i=1}^N \sigma_i u_i(\bar{\mathbf{x}}_1) v_i(\mathbf{x}) - \sum_{i=1}^N \sigma_i u_i(\bar{\mathbf{x}}_2) v_i(\mathbf{x}) \right)^2 \\
&= \sum_{\mathbf{x} \in \mathcal{X}} \left( \sum_{i=1}^N \sigma_i (u_i(\bar{\mathbf{x}}_1) - u_i(\bar{\mathbf{x}}_2)) v_i(\mathbf{x}) \right)^2 \\
&= \sum_{\mathbf{x} \in \mathcal{X}} \sum_{i, i'} \sigma_i v_i(\mathbf{x}) \sigma_{i'} v_{i'}(\mathbf{x}) (u_i(\bar{\mathbf{x}}_1) - u_i(\bar{\mathbf{x}}_2)) (u_{i'}(\bar{\mathbf{x}}_1) - u_{i'}(\bar{\mathbf{x}}_2)) \\
&= \sum_{i, i'} \sigma_i \sigma_{i'} (u_i(\bar{\mathbf{x}}_1) - u_i(\bar{\mathbf{x}}_2)) (u_{i'}(\bar{\mathbf{x}}_1) - u_{i'}(\bar{\mathbf{x}}_2)) \sum_{\mathbf{x} \in \mathcal{X}} v_i(\mathbf{x}) v_{i'}(\mathbf{x}) \\
&\stackrel{(1)}{=} \sum_{i, i'} \sigma_i \sigma_{i'} (u_i(\bar{\mathbf{x}}_1) - u_i(\bar{\mathbf{x}}_2)) (u_{i'}(\bar{\mathbf{x}}_1) - u_{i'}(\bar{\mathbf{x}}_2)) \delta_{i, i'} \\
&= \sum_{i=1}^N \sigma_i^2 (u_i(\bar{\mathbf{x}}_1) - u_i(\bar{\mathbf{x}}_2))^2
\end{aligned}$$

(1) is due to the orthogonality of singular vectors. And  $g(\bar{\mathbf{x}})$  takes the following form:

$$g(\bar{\mathbf{x}}) = Q [\sigma_1^2 u_1(\mathbf{x}), \sigma_2^2 u_2(\mathbf{x}), \dots, \sigma_k^2 u_k(\mathbf{x})]^\top.$$

Thus,

$$\begin{aligned}
\|g(\bar{\mathbf{x}}_1) - g(\bar{\mathbf{x}}_2)\|_{\Sigma_k}^2 &= \sum_{i=1}^k \sigma_i^2 (u_i(\bar{\mathbf{x}}_1) - u_i(\bar{\mathbf{x}}_2))^2 \\
&= d_{\text{w-aug}}^2(\bar{\mathbf{x}}_1, \bar{\mathbf{x}}_2) - \sum_{i=k+1}^N \sigma_i^2 (u_i(\bar{\mathbf{x}}_1) - u_i(\bar{\mathbf{x}}_2))^2 \quad (\leq d_{\text{w-aug}}^2(\bar{\mathbf{x}}_1, \bar{\mathbf{x}}_2)) \\
&\geq d_{\text{w-aug}}^2(\bar{\mathbf{x}}_1, \bar{\mathbf{x}}_2) - \sigma_{k+1}^2 \sum_{i=1}^N (u_i(\bar{\mathbf{x}}_1) - u_i(\bar{\mathbf{x}}_2))^2 \\
&= d_{\text{w-aug}}^2(\bar{\mathbf{x}}_1, \bar{\mathbf{x}}_2) - 2\sigma_{k+1}^2 (1 - \delta_{\bar{\mathbf{x}}_1 \bar{\mathbf{x}}_2})
\end{aligned}$$

## E Ablation Study on Parameter $\alpha$ and $K$

We conduct ablation experiments on the parameter  $\alpha$  and  $K$ .  $\alpha$  is the trade-off parameter between partial contrastive principal component loss and projection loss Equation (9).  $K$  act as the noise strength for CPCL-A, which replace  $N$  in Equation (5).

Figure 4 shows the effect of  $\alpha$  and  $K$  on different benchmarks. It can be seen that  $\alpha$  is necessary to improve the performance of CPCL-A. A certain value of  $\alpha$  helps the model achieve better results. However, a too large value of  $\alpha$  degrades the performance. The same phenomenon is the same on  $K$ .



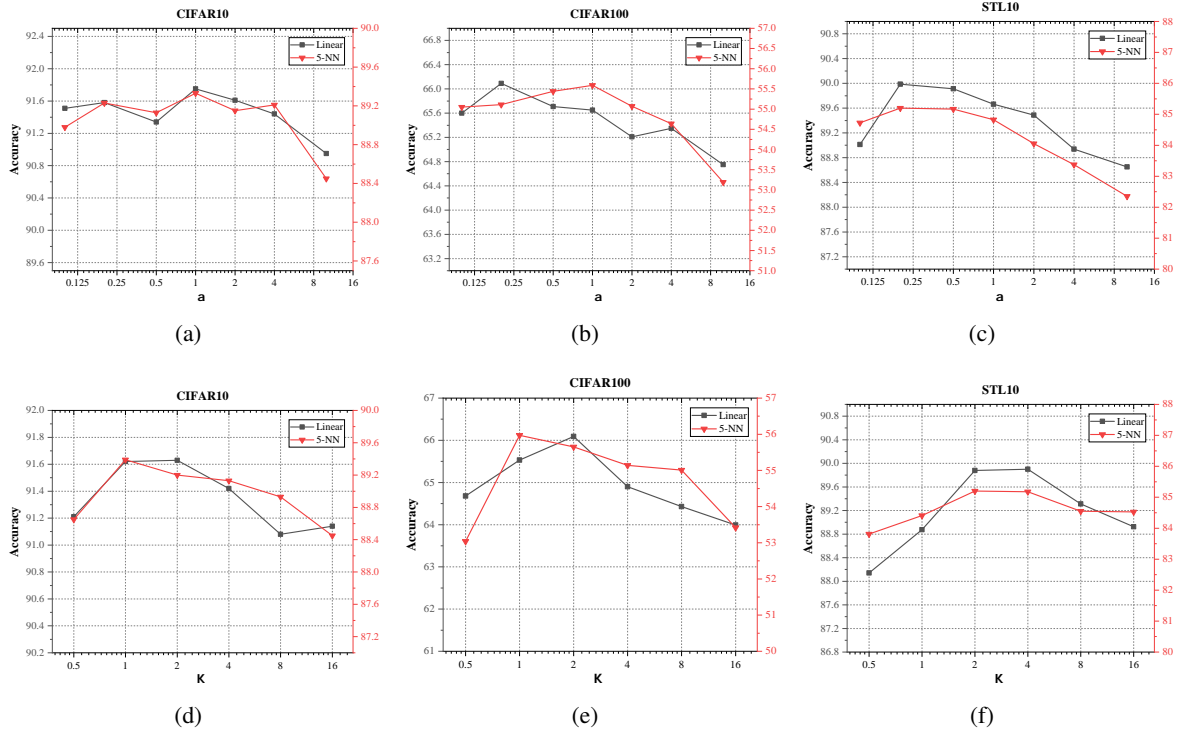


Figure 4: Ablation studies on the effect of  $\alpha$  and  $K$ . We report linear classification and 5-nearest neighbor accuracy on different datasets with the ResNet-18 encoder. The upper 3 figures illustrate the effect of  $\alpha$  on 3 different datasets. The lower 3 figures illustrate the performance v.s.  $K$ .

## F Comparison of Nearest Neighbors

We random select 8 samples from the validation set of ImageNet-100 [3]. Then we use the encoder learned by our CPCL method and SimCLR [5] to extract features and investigate their nearest neighbors of them. The left-most column displays the selected samples and the following columns show the 5 nearest neighbors. The samples that are labeled as the different classes have been marked by the red box. We also annotate the distance between the samples and their nearest neighbors. First, we can see that even though utilizing the augmentation in a different way, CPCL achieves similar results as traditional contrastive learning. Both of them can learn semantically meaningful embeddings. However, we can see that CPCL tends to learn embeddings that pull together images that are similar in the input space, *i.e.*, creating similar augmentation, while SimCLR sometimes has neighbors that seem different.

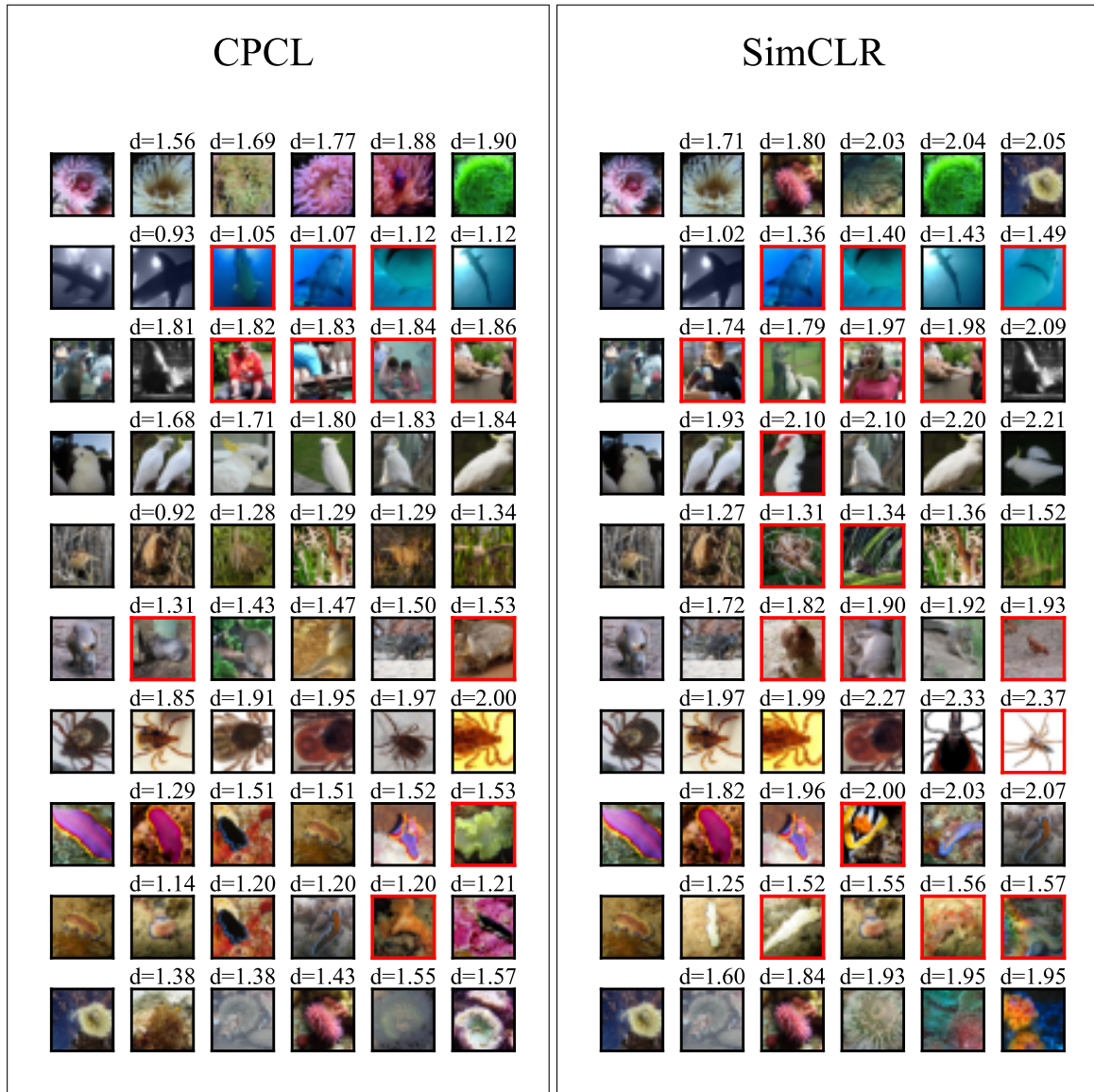


Figure 5: The 5 nearest neighbors of selected samples in the embedding space of CPCL and SimCLR. Images are taken from the validation set of ImageNet-100. Distances between selected samples and their nearest neighbors are annotated above each picture. We can see that the embeddings learned by CPCL tend to pull together images that are similar in the input space, *i.e.*, creating similar augmentation. While SimCLR sometimes has neighbors that seem different.